A Novel Algorithm for Forest Height Estimation from PolInSAR Image

Nghia Pham Minh and Bin Zou

Dept. of Information Engineering, Harbin Institute of Technology, Harbin, China
nghiapmlqdu@gmail.com, zoubin@hit.edu.cnl

Abstract

Forest height is important information for many forest management activities and is a critical parameter in models of ecosystem procedures. Recently, there have been plenty of researches on the retrieval of forest height by single baseline PolInSAR such as the ESPRIT method, three-stage inversion but the methods tend to underestimate the forest height due to attenuation of the electromagnetic waves in the ground medium and vary widely in their sensitivities. This paper proposes a novel algorithm to retrieve forest height using an adaptive scattering model-based decomposition technique with PolInSAR data. The object is to describe each interferometry cross correlation as a sum of contributions corresponding to odd bounce, double bounce and volume scattering processes. This algorithm enables the retrieval not only of the vegetation parameters but also of the magnitude associated with each mechanism. Another advantage of the proposed algorithm is that it makes use of all the information provided by the covariance matrix, which remains unachieved in the previous model-based decompositions. The proposed algorithm has been tested with simulated data from PolSARProSim software and spaceborne data from a test site. Experimental results indicate that accuracy of the forest height estimation can be enhanced by the proposed algorithm.

Keywords: *PolInSAR, target decomposition, adaptive decomposition, coherence amplitude, forest height estimation*

1. Introduction

Forest canopy structure is a key determinant of forest ecosystem processes, and its measurement is essential for ecosystem monitoring, modeling and management [13, 18]. Estimation of height forest by means of polarimetric interferometric synthetic aperture radar (PolInSAR) observations is one of the most promising applications in the field of active microwave remote sensing. Several techniques have been proposed for the forest height estimation using single baseline PolInSAR image such as ESPRIT method [16, 19], three-stage inversion [10]. The ESPRIT technique can detect local scattering centers corresponding to the canopy top and ground in the forest area but detection accuracy of the technique becomes worse for dense forest regions due to strong volume scattering component. The three-stage method requires multiple parameter least-square estimation which is complex and often becomes ill-conditioned. For that reason, we propose using model-based decomposition technique for forest height estimation from PolInSAR image. Recently, many decomposition techniques have been proposed for polarimetric synthetic aperture radar (PolSAR) image analysis such as Freeman and Durden decomposition [2], Yamaguchi four-component decomposition [9], Cloude-Pottier decomposition [12], most of them expressed the average

mechanism as the sum of independent components with each resolution cell, which allows the identification and separation of scattering mechanisms in the polarization signature for purposes of classification and recognition. However, these decomposition techniques present two major flaws in its definition. In first place, the volume scattering terms is assumed the scattering reflection symmetry and the same volume scattering model for all pixels. In second place, the number of independent observables is limited so they adopt some assumption to remove ambiguity and determine the unique solution, as analyzed in [2, 3]. The assumptions often cause negative power in the decomposed mechanisms especially for forest areas where volume scattering component is dominant [11]. Recently, Arri [5, 6] proposed a general volume model and adaptive model-based decomposition to overcome these limitations. The model does not require any geophysical media symmetry assumption but in order to estimate parameters of the model somewhat complicated computation is required.

We show that the polarimetric parameters extracted by using different polarimetric decomposition techniques are related to the physical characteristic of a target whereas the interferometric information can reflect the geometry structure and complexity of the observed objects. Therefore, one general solution to overcome restrictions of decomposition technique has been to increase the number of observables, as proposed with the polarimetric SAR interferometric (PolInSAR) technique [4]. In principle, using PolInSAR is possible to identify not only the scattering mechanisms but also their positions or distributions along the vertical dimension of the land cover structure [14, 17]. However, these methods tend to underestimate the forest height and are not able to distinguish between odd-bounce and double bounce scattering.

In this paper, we propose an adaptive model-based decomposition technique for single frequency single baseline PolInSAR measurement. In this algorithm, we apply a generalized volume component as in [5] that it can be characterized by two parameters: a mean orientation angle and a degree of randomness. Then, we suggest that the reference volume scattering covariance can be used to determine the best fit parameters to express general volume scattering covariance matrix. The proposed method is executed following three steps. Firstly, the ground topography and canopy phase are estimated by the adaptive decomposition technique. Secondly, the forest height is estimated by phase differencing method. Finally, the height is compensated by the coherence amplitude approach. The propose method enable estimate not only of power contribution from soil and volume but also their location along the vertical coordinate. Experimental results show that accuracy of the forest height can be improved by this scheme.

The organization of this paper is as follows. In Section 2, we present the elementary scattering mechanisms for polarimetric SAR interferometric observations. The retrieval of forest height from the proposed algorithm is delivered in Section 3. The experimental results of the parametric inversion with simulated data and space-borne data are presented and discussed in Section 4. Finally, the conclusion and future work are drawn in Section 5.

2. Elementary Scattering Mechanisms for PoInSAR Data

For forest observations, the backscattered waves can be considered as the sum of the three components shown in Figure 1. The main scattering contributions explicitly denoted are surface (s), double-bounce (d) and volume (v) as proposed by Freeman and Durden [2].

Hence, the starting point is the definition of the target vector for both ends of the baseline. A full polarimetric interferometric system are measured for each resolution element in the scene from two slightly different look angles, two scattering matrices $[S_1]$ and $[S_2]$. In the

case of backscattering in a reciprocal medium, the 3-D lexicographic scattering vector $\vec{k}_{L_1}$ and $\vec{k}_{L_2}$ are given by:

$$\vec{k}_{L_1} = \left[S_{1hh}, \sqrt{2}S_{1hv}, S_{1vv}\right]^T$$
$$\vec{k}_{L_2} = \left[S_{2hh}, \sqrt{2}S_{2hv}, S_{2vv}\right]^T \quad (1)$$

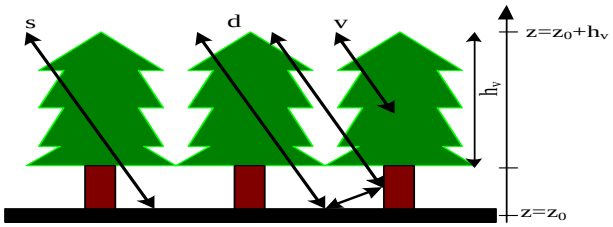

Figure 1. Three scattering contributions used in model-based decomposition

The complete information measured by the SAR system can be represented in the form of three 3x3 complex matrices $[C_{11}]$, $[C_{12}]$ and $[C_{22}]$ formed using the outer products of the target vectors $\vec{k}_{L_1}$ and $\vec{k}_{L_2}$ as follows

$$[C_{11}] = \langle \vec{k}_{L_1} \vec{k}_{L_1}^{*T} \rangle$$
$$[C_{22}] = \langle \vec{k}_{L_2} \vec{k}_{L_2}^{*T} \rangle \quad (2)$$
$$[C_{12}] = \langle \vec{k}_{L_1} \vec{k}_{L_2}^{*T} \rangle$$

Where $\langle \cdot \rangle$ denotes the ensemble average in the data processing, and * denotes the complex conjugation. $[C_{11}]$ and $[C_{22}]$ are the conventional Hermitian polarimetric covariance matrices, which describe the polarimetric properties for each individual image separately, while $[C_{12}]$ is a non-Hermitian complex matrix which contains polarimetric and interferometric information. The cross correlation matrix $[C_{12}]$ is presented as follow

$$[C_{12}] = \begin{bmatrix} \langle S_{1hh} S_{2hh}^* \rangle & \langle \sqrt{2} S_{1hh} S_{2hv}^* \rangle & \langle S_{1hh} S_{2vv}^* \rangle \\ \langle \sqrt{2} S_{1hv} S_{2hh}^* \rangle & \langle 2 S_{1hv} S_{2hv}^* \rangle & \langle \sqrt{2} S_{1hv} S_{2vv}^* \rangle \\ \langle S_{1vv} S_{2hh}^* \rangle & \langle \sqrt{2} S_{1vv} S_{2hv}^* \rangle & \langle S_{1vv} S_{2vv}^* \rangle \end{bmatrix} \quad (3)$$

The cross correlation matrix $[C_{12}]$ will be expressed as the sum of three matrices accounting for the contributions of single bounce $[C_S]$, double bounce $[C_D]$ and volume scattering $[C_V]$ as follow

$$[C_{12}] = [C_S] + [C_D] + [C_V] \quad (4)$$

In the next section, the three scattering mechanisms to polarimetric interferometric observables are analyzed. Note that, as already demonstrated in [2], a null correlation between co-polar and cross-polar channels will be assumed.

2.1. Single bounce scattering model

The single bounce scattering model is presented by the first order Bragg surface scatter, plate, sphere and triple-bounce scattering modeling slightly rough surface scattering in which the cross-polarized component is negligible. Additionally, the Bragg model states that

$|VV| > |HH|$. Hence, Bragg scattering parameters for master and slave images, which actually depend on the surface complex permittivity and incidence angle. The amplitude of the scattering coefficient does not change for both images, except the difference in the phase term. This phase term will have two contributions: the difference due to the complex scattering coefficient in the case of using different polarization for master and slave image $\psi_{hv} = \psi_h - \psi_v$ and the interferometric phase related with position in the vertical coordinate ϕ_S. Note that, the phase of direct scattering will not necessarily locate at ground level. The scattering matrix of Bragg surface for master and slave images can be expressed in simplified form as

$$[S_S^1] = \begin{bmatrix} S_{1hh} & 0 \\ 0 & S_{1vv} \end{bmatrix} \quad \text{and} \quad [S_S^2] = \begin{bmatrix} S_{2hh}e^{-j\phi_S} & 0 \\ 0 & S_{2vv}e^{-j\phi_S} \end{bmatrix} \tag{5}$$

Where ϕ_S denotes the interferometric phase for the direct scattering. We assume that the same phase of co-polarized for both images. In this case, the covariance matrix for the single bounce model is represented as

$$[C_S] = F_S \begin{bmatrix} |\beta|^2 & 0 & \beta \\ 0 & 0 & 0 \\ \beta^* & 0 & 1 \end{bmatrix} \tag{6}$$

Where F_S and β are defined as:

$$F_S = |S_{vv}|^2 e^{j\phi_S}$$
$$\beta = \frac{|S_{hh}|}{|S_{vv}|} e^{j\psi_{hv}} \tag{7}$$

2.2. Double bounce scattering model

The double bounce scattering component is modeled by scattering from a dihedral corner reflector, including a double scattering interaction between the ground and tree-trunk or stem, where the reflector surface can be made of different dielectric materials. This contribution is modeled in (8) for both ends of the baseline [4, 12]

$$[S_D^i] = \begin{bmatrix} R_{gh}R_{th}e^{-j2\gamma_{hi}} & 0 \\ 0 & R_{gv}R_{tv}e^{-j2\gamma_{vi}} \end{bmatrix} \tag{8}$$

where i=1,2 correspond to both master and slave images. R_{gh} and R_{gv} are the horizontal and vertical Fresnel reflection coefficients of the ground surface. Similarly, the vertical trunk surface has reflection coefficients R_{th} and R_{tv} for horizontal and vertical polarizations, respectively. These coefficients are assumed to be equal for master and slave images. The complex coefficients γ_{hi} and γ_{vi} accounting for wave propagation processing. These terms are divided in two parts considering attenuation ρ and phase propagation ψ. We assume that the attenuation for master and slave images of the interferometric pair and both polarization are same. For instance, the complex coefficient difference for both ends of the baseline is expressed as

$$2(\gamma_{v1} - \gamma_{v2}) = 2\left(\frac{\psi_{v1}}{2} + j\frac{\sigma_{v1}}{2} - \frac{\psi_{v2}}{2} - j\frac{\sigma_2}{2}\right) = -\psi_{hv} - \phi_D \tag{9}$$

where ϕ_D, $\psi_{hv}$are the interferometric phase for the double bounce scattering component and polarization phase difference, respectively. Scattering matrices in (8) yields a covariance matrix for the double bounce model is given by

$$[C_D] = F_D \begin{bmatrix} |\alpha|^2 & 0 & \alpha \\ 0 & 0 & 0 \\ \alpha^* & 0 & 1 \end{bmatrix} \tag{10}$$

Where F_D and α are defined as

$$F_D = |R_{GV} R_{TV}|^2 e^{j\phi_D}$$
$$\alpha = \frac{R_{GH} R_{TH}}{R_{GV} R_{TV}} e^{j\psi_{HV}} \tag{11}$$

2.3. General volume scattering model

The volume scattering is direct volume scattering from the top layer of forest model. By assuming this layer has azimuthal symmetry, so the scattering from canopy forest can be reasonably characterized by a cloud of randomly oriented infinitely thin cylinder [5, 9]. The scattering matrix for particle in the random volume is [1, 12]

$$\left[S_{vol}^i\right] = \begin{bmatrix} S_{hi} & 0 \\ 0 & S_{vi} \end{bmatrix} \tag{12}$$

where i=1,2, which refers to each end of the baseline.

The scattering matrix of each particle inside the canopy layer when rotated by angle around the radar line of sight, becomes

$$\left[S_{vol}^i(\theta)\right] = \begin{bmatrix} cos\theta & sin\theta \\ -sin\theta & cos\theta \end{bmatrix} \left[S_{vol}^i\right] \begin{bmatrix} cos\theta & -sin\theta \\ sin\theta & cos\theta \end{bmatrix} \tag{13}$$

In the theoretical modeling of volume scattering, a cloud of randomly oriented dipoles in implemented with a uniform probability function for the orientation angles. However, for vegetated areas where vertical structure seems to be rather dominant, the scattering from tree trunks and branches display a non-uniform angle distribution. Assuming a volume with a *n*th power cosine-squared distribution of orientation with probability density function as [5, 6]. The parameter *n* ranges from zero to infinity. In practice, there is little difference between distributions with values of *n* larger than about 20 or so. It can be shown that the standard deviation σ can be evaluated in terms of *n* as [6]. The standard deviation σ varies from a range between 0 and 0.91. It changes with the corresponding change in distribution function from delta to uniform distribution function for the vegetation orientation angles.

Assuming that the dipole or the thin cylinder scatters are randomly about the radar look direction, the volume scattering covariance matrix can be rewritten as :

$$\langle [C_V(\theta_0, \sigma)] \rangle = [C_\alpha] + p(\sigma)\left[C_\beta(2\theta_0)\right] + q(\sigma)\left[C_\gamma(4\theta_0)\right] \tag{14}$$

where θ_0 is the mean orientation angle of the dipoles. The coefficient $p(\sigma)$ and $q(\sigma)$ are characterized by sixth-order polynomials as in [5, 6]. The basic covariance matrices $[C_\alpha]$, $\left[C_\beta\right]$ and $\left[C_\gamma\right]$ are represented as:

$$[C_\alpha] = \frac{1}{8}\begin{bmatrix} 3 & 0 & 1 \\ 0 & 2 & 0 \\ 1 & 0 & 3 \end{bmatrix}$$

$$\left[C_\beta(2\theta_0)\right] = \frac{1}{8}\begin{bmatrix} -2cos2\theta_0 & \sqrt{2}sin2\theta_0 & 0 \\ \sqrt{2}sin2\theta_0 & 0 & \sqrt{2}sin2\theta_0 \\ 0 & \sqrt{2}sin2\theta_0 & 2cos2\theta_0 \end{bmatrix} \quad (15)$$

$$\left[C_\gamma(4\theta_0)\right] = \frac{1}{8}\begin{bmatrix} cos4\theta_0 & -\sqrt{2}sin4\theta_0 & -cos4\theta_0 \\ -\sqrt{2}sin4\theta_0 & -2cos4\theta_0 & \sqrt{2}sin4\theta_0 \\ -cos4\theta_0 & \sqrt{2}sin4\theta_0 & cos4\theta_0 \end{bmatrix}$$

3. The Forest Height Estimation Using Hybrid Algorithm

3.1. Adaptive model-based decomposition algorithm extracting forest height

In this section we propose the algorithm for the estimation of the forest height using single baseline polarimetric interferometric SAR. One of the simplest approaches to forest height estimation is to use the phase difference between interferogram as a direct estimate of forest height [1, 10]. In general terms we then estimate the phase in two scattering components: the first is the volume scattering only which has a phase center near the top of layer, and the second is surface scattering dominated which has a phase center near the ground. In this paper, forest height estimation can be extracted by an adaptive model-based decomposition algorithm [21].

Based upon the generalized model for volume scattering, we shall develop the adaptive decomposition algorithm in this section. Simple replacement of the volume scattering term in (4) by (14) provides the new decomposition model as

$$[C_{12}] = F_V[C_V(\theta_0, \sigma)] + F_S[C_S] + F_D[C_D] \quad (16)$$

Firstly, the above equation is used to find the volume scattering covariance matrix. In the case of vegetation model, the co-polar and cross-polar responses are uncorrelated and cross-polar response is generated by volume scatters [6, 11]. Consequently, we employed a generalized volume scattering mechanism model in (17) using geophysical media symmetry as a reference volume scattering model. Under the reflection symmetry assumption for reciprocal medial, the covariance matrix for backscatter, regardless of actual physical scattering mechanism (volume or surface), obeys the following expression [7]

$$\left[C_{V\_refer}\right] = \frac{1}{\frac{3}{2}(1+\delta)-\sqrt{\delta}/3}\begin{bmatrix} \delta & 0 & \sqrt{\delta}/3 \\ 0 & \frac{1+\delta}{2}-\frac{\sqrt{\delta}}{3} & 0 \\ \sqrt{\delta}/3 & 0 & 1 \end{bmatrix} \quad (17)$$

With $\delta = \langle|S_{HH}|^2\rangle/\langle|S_{VV}|^2\rangle$

In this paper, we suggest that the reference volume scattering covariance can be used to determine the best fit parameters to express general volume scattering covariance matrix. At first we calculate the reference matrix $C_{V-refer}$ as in (17). Secondly, we implement finding the volume scattering covariance matrix so that $C_V(\theta_0, \sigma)$ approximates to the reference volume scattering covariance matrix $C_{V-refer}$ by varying randomness σ and mean orientation angle θ_0 for their entire range. These parameter sets are equivalent to a best fit under condition that subtraction of general volume covariance matrix and reference volume covariance matrix becomes zero. Finally, we repeat both above step for each pixel in image.

The algorithm is summarized in Figure 2. When the generalized volume covariance matrix is selected, we can calculate F_V as :

$$F_V = |f_v|e^{j\phi_v} = \frac{C_{12}(2,2)}{C_V(2,2)} \tag{18}$$

Power of volume scattering component can be derived by the coefficient f_v and the canopy phase ϕ_V can be obtained in (18). Following the proposed algorithm for polarimetric interferometric data, when the proper $[C_V]$, ϕ_v and f_v are selected, we can remove the volume scattering component from the original covariance matrices. The remainder matrix is presented as:

$$[C_{remainder}] = [C_D] + [C_S] = \begin{bmatrix} |\alpha|^2 F_D + |\beta|^2 F_S & 0 & \alpha F_D + \beta F_S \\ 0 & 0 & 0 \\ \alpha^* F_D + \beta^* F_S & 0 & F_D + F_S \end{bmatrix} \tag{19}$$

As can be seen, in matrix $[C_{remainder}]$ there appear four complex unknowns α, β, F_D and F_S and four complex observables, since $C_{remainder}(1,3) \neq C_{remainder}(3,1)$. This formulation leads to a determined nonlinear equation system. Therefore, to determine the rest of unknown parameters F_D, F_S, α and β simultaneously, an ESPRIT algorithm is implemented. In addition, magnitude of estimated the complex eigenvalues correspond to complex coherence of local scatters by the ESPRIT analysis for (18).

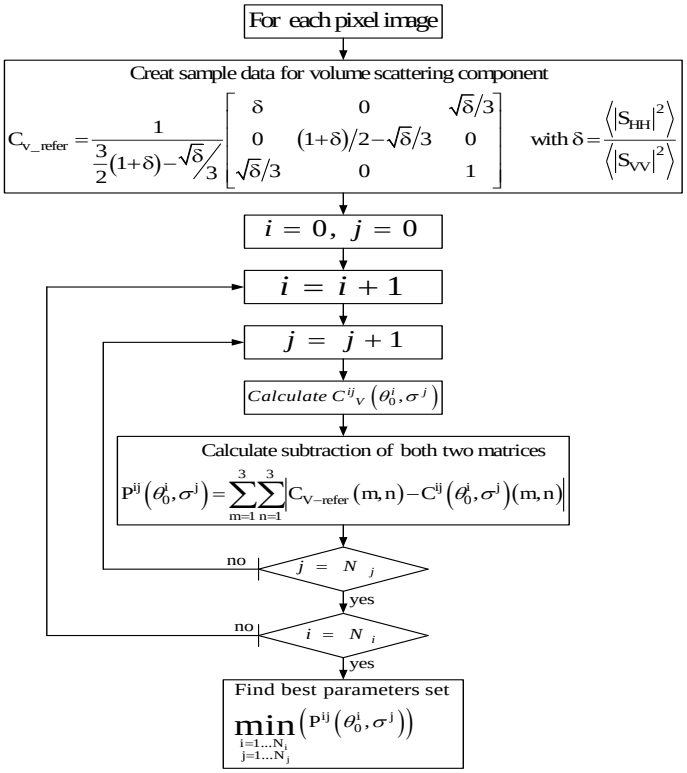

Figure 2. Adaptive model-based decomposition algorithm for single pixel

In order to remove ambiguity and improve the accuracy of each power component, we employ the modified ESPRIT-based PolInSAR [3]. If the single bounce is dominant the parameters F_D, F_S, α and β are expressed as:

$$\begin{aligned} \beta &= \frac{e_1(1) - \sqrt{\lambda_r} k e_1(3) e^{-j\xi}}{e_2(1) - \sqrt{\lambda_r} k e_2(3) e^{-j\xi}} \\ \alpha &= \frac{e_1(1) + \sqrt{\lambda_r} k^{-1} e_1(3) e^{-j\xi}}{e_2(1) + \sqrt{\lambda_r} k^{-1} e_2(3) e^{-j\xi}} \\ F_S &= \left\{ e_2(1) - \sqrt{\lambda_r} k e_2(3) e^{-j\xi} \right\}^2 \\ F_D &= \left\{ e_2(1) + \sqrt{\lambda_r} k^{-1} e_2(3) e^{-j\xi} \right\}^2 \\ \lambda_r &= \lambda_2 / \lambda_1 \end{aligned} \tag{20}$$

Where $\lambda_i$and $e_i$are the eigenvalue and corresponding eigenvector of the *i*th component of $C_{remainder}$ matrix. The coefficients k and ξ are elements of unitary matrix as in [3]. Finally, we choose the argument of coefficient F_S which corresponds to surface topography to be employed into forest height estimation. Then the forest height by phase differencing can be expressed as:

$$h_v = \frac{\phi_v - \phi_0}{k_z} \tag{21}$$

Where k_z, ϕ_V, ϕ_0 are vertical wavenumber, canopy phase and surface phase respectively.

We show that, this algorithm requires no further assumption or checks to determine which canopy model to use in the decomposition technique. We propose the algorithm because it allows simple implementation with reasonable flexibility and not complex computation. The proposed algorithm is optimum for the forest area. However, it has been applied to other types such as bare surface and urban areas.

3.2. The coherence amplitude method

In the case of forest model the propagation through the volume is independent of polarization. Consequently, the volume only complex coherence $\tilde{\gamma}_v$ becomes independent of polarization [15].

$$\tilde{\gamma}_v(h_v, \sigma) = \frac{\int_0^{h_v} e^{(2\sigma z')/cos\theta_0} e^{jk_z z'} dz'}{\int_0^{h_v} e^{(2\sigma z')/cos\theta_0} dz'} \tag{22}$$

Where k_z, θ_0 are vertical wavenumber and incidence angle, respectively. In [10], Cloude proposed three-stage inversion in vegetation parameters estimation. In particular, assuming the extinction approaches zero, the volume only complex coherence $\tilde{\gamma}_v(h_v, \sigma)$ is the function which can only contain height. Then the volume complex coherence $\tilde{\gamma}_v(h_v)$ is expressed by:

$$\tilde{\gamma}_v(h_v) = \lim_{\sigma \to 0} \frac{2\sigma \int_0^{h_v} e^{(2\sigma z')/cos\theta_0} e^{jk_z z'} dz'}{cos\theta_0 \left(e^{(2\sigma h_v)/cos\theta_0} - 1\right)} = e^{jk_z h_v/2} sinc(k_z h_v/2) \tag{23}$$

Equation (23) shows that the SINC model is that the coherence amplitude falls with increasing height and hence phase variance increases with h_v. Then we can use estimate of measure coherence amplitude to estimate height (for a known baseline). The volume only coherence complex $\tilde{\gamma}_v$ can be replaced with $\tilde{\gamma}_v(\omega_v)$ so the forest height can be written as

$$h_v = \frac{2 arcsinc(|\tilde{\gamma}_v(\omega_v)|)}{k_z} \tag{24}$$

In particular, for short baseline we can expand h_v function as:

$$h_v \approx \frac{\pi - arcsin(|\tilde{\gamma}_v(\omega_v)|^{0.8})}{k_z} \quad (25)$$

The coherence amplitude in equation (25) is sensitive to variation in the vertical structure of forest and is generally applied to compensate the underestimated height.

3.3. Estimation of forest height

In order to estimate height, we first use this height which is estimated by the adaptive model-based decomposition algorithm, exactly as proposed in equation (21). However, the canopy phase can lie anywhere between halfway and top of the layer, and hence in general the true height is underestimated. To progress, one key idea is that this error can be at least partly compensated by employing a coherence amplitude correction term. Finally, by combining these two terms with a scaling parameter η, we then obtain an approximate algorithm that can compensate variation in structure, as shown in equation (26):

$$h_v = \frac{\phi_v - \phi_0}{k_z} + \eta \frac{\pi - 2arcsin(|\tilde{\gamma}_v(\omega_v)|^{0.8})}{k_z} \quad (26)$$

The first term represents the phase coherence while the second term is the coherence amplitude correction. This expression has the right kind of behavior in two important special cases. If the medium has a uniform structure function the first term will give half the height but the second will then also obtain half the true height (if we set $\eta=0.5$). At the other extreme, if the structure function in the volume channel is localized near top of the layer, then phase height will give the true height, and second term will approach zero that reason the weight set as $\eta=0$. To reduce the error from change of extinction coefficient and the vertical structure, we select $\eta=0.4$ [8].

4. Experimental Results and Discussion

In this section, the proof of the algorithm concept proposed in Section 3 is addressed. To illustrate the technique, we apply the adaptive model-based decomposition algorithm to a data set acquired from PolSARProSim software by Mark L. Williams [20], as well as L-band image pair of Tien-shan test site by the SIR-C/X-SAR system

4.1. Simulated Data

The proposed algorithm has been first test a simulated RVoG scenario, named as HEDE in the PolSARProSim software, at 1.3GHz and at 30 degree angle of incidence considering different soil conditions and averaging window sizes. The interferometer is operated at 10.6m horizontal and -6.1m vertical baseline. The stand height 10m, and it is located on a 0.1% ground azimuth and 0.2% ground range slope. The forest stand occupies a 0.7854 Ha area and stand density is 360stem/Ha. Azimuth and slant range resolution are 1.0m and 0.5m, respectively.

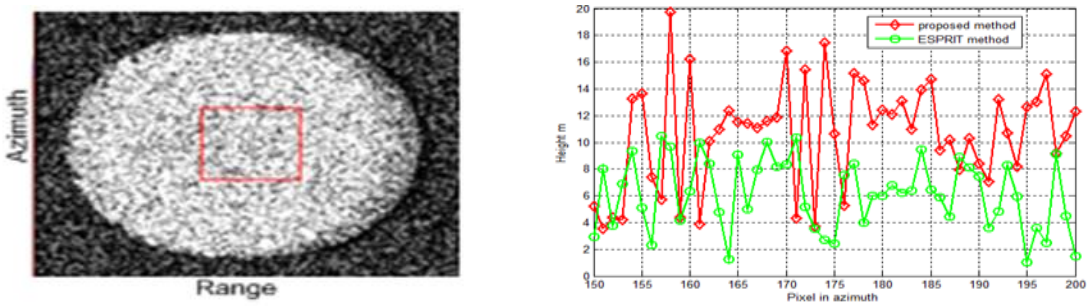

(a) **(b)**

Figure 3. Simulated data and experimental results. Figure 3(a) shows HH amplitude image of the simulated data. Figure 3(b) shows height result comparison

Figure 3(a) shows HH amplitude image of the simulated data. Figure 3(b) is a histogram of the height estimation of proposed algorithm compared with the ESPRIT approach. Compared with the actual 10m tree height, Table 1 indicates the proposed approach is more accurate. The estimation of forest height using ESPRIT approach is the absolution of the difference between the effective scattering phase centers of surface topography and canopy layer. Therefore, in the ESPRIT approach the poor performance is caused by the closer two phase centers.

Table 1. Comparison between ESPRIT Model and Proposed Approach

	Height average (m)	average errors (m)	RMSE (m)
ESPRIT method	6.3082	3.6198	0.8496
Proposed approach	9.3228	0.7672	0.1512

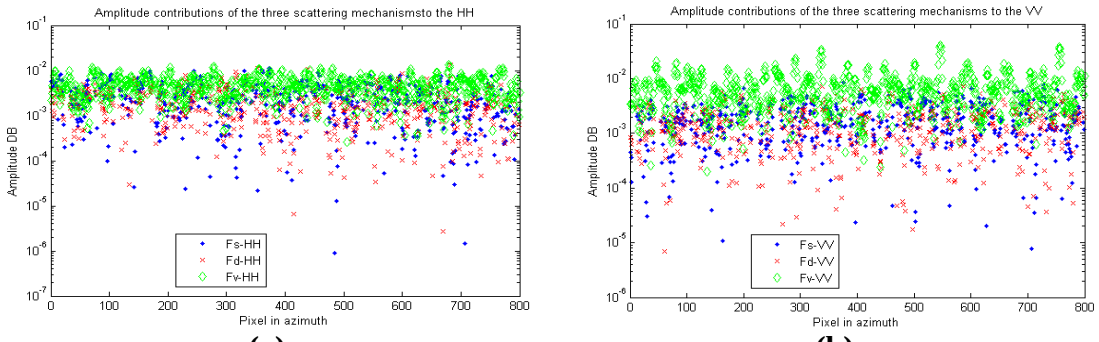

(a) **(b)**

Figure 4. Amplitude contributions of three scattering mechanisms to (a) HH and (b) VV with highest roughness

Figure 4 corresponds to the amplitude of the three scattering mechanism contributing to the HH (figure 4(a)) and VV (Figure 4(b)) channel. As shown, the amplitude response is dominated by the volume scattering but there are certain areas where the

single scattering component is also remarkable. In addition, the double-bounce scattering component is low for the VV correlation (as predicted by theory), and it is not dominant in the HH channel due to surface has a highest roughness.

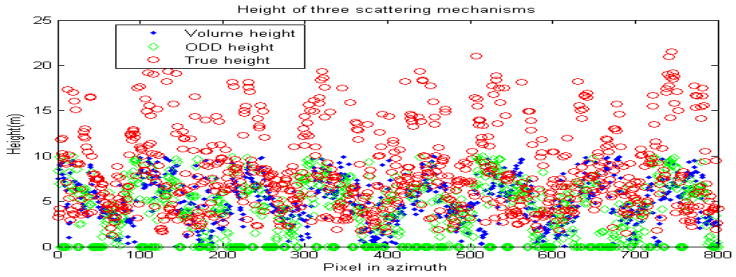

Figure 5. The height estimates for the scattering components.

The height estimates of the volume scattering and odd-bounce scattering component are shown in Figure 5. Almost all height estimates of odd-single scattering are approximate zero expect a little values have height greater due to the soil roughness, moisture conditions and terrain slope. This figure shows that the actual forest heights are quite well retrieved, except for pixels around 90, 190, 400, 600 and 700. Likewise, the heights are very accurately estimated.

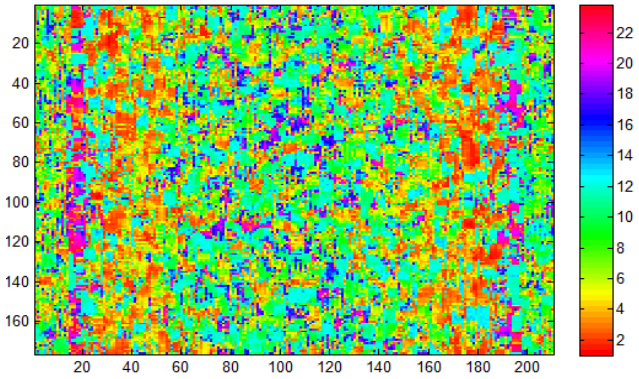

Figure 6. Forest height is estimated by proposed algorithm

The result of the proposed method is shown in Figure 6. In this figure it is shown that almost the peak differential of the height is located at 10m approximately. The forest height estimation between the azimuth 17-20 and 195-200 pixels are overestimated less than 22m. The real effective tree height will be higher than these values. Hence, we can say that the results are acceptable. Consequently, the proposed method provides relative accuracy with small error, and is more accurate for vertical structural variations.

Changes in the scene parameters can be noticed by means of the proposed decomposition algorithm. Figure 7 represents the amplitude contributions of the three scattering mechanism to HH and VV interferometry channels when surface has the lowest roughness. The rest of parameters remain unchanged. We show that the volume contribution does not vary, as expected. By comparing Figures 4 and 7, one can observe that for this data set the algorithm accounts for the differences on the surface condition

by means of the contributions of double-bounce to VV and HH channels. The amplitude contribution of the double-bounce has just low value for the VV channel. However, the double-bounce contribution increases and becomes dominant in some areas due to interaction between smooth surface and trunks (such as at some around pixels 100, 190, 300, 400).

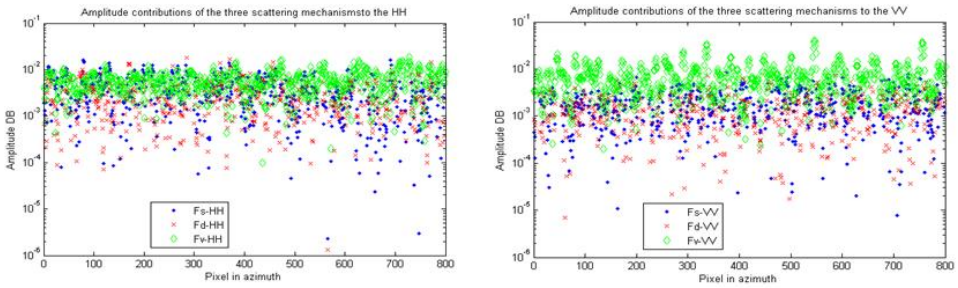

(a) (b)

Figure 7. Amplitude contributions of three scattering mechanisms to (a) HH and (b) VV with lowest roughness

4.2. Spaceborne Data

Next, we have also tested the proposed algorithm with space-borne data. In the present study, the data used consists of two SIR-C single look complex (SLC) image pair of the Tien-shan test site by the SIR-C system. This region has a mixed forestry, road and agricultural area. They consist of quad-pol interferometric data at L band with a 24.569 degree angle of incidence and 13m baseline. Figure 8(a) is the optical image of the test site, Figure 8(b) is the HV amplitude image of test area for evaluation as forest and Figure 8(c) is a composite image of the test site in the Pauli basis, with 500 pixels in range and 500 pixels in azimuth.

The analysis has been performed on the azimuth transect. Along this transect, we can identify three types of scenes: red areas denote bare surface like agriculture and road, green areas represent forest.

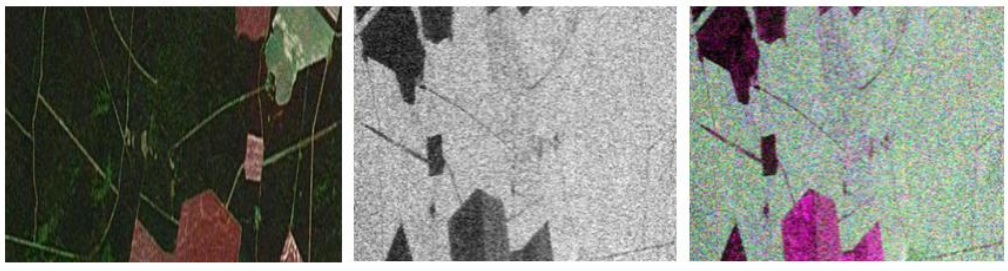

(a) (b) (c)

Figure 8. Test site in Tien-Shan: (a) Optical image (b) HV amplitude image (c) Pauli decomposition of test site

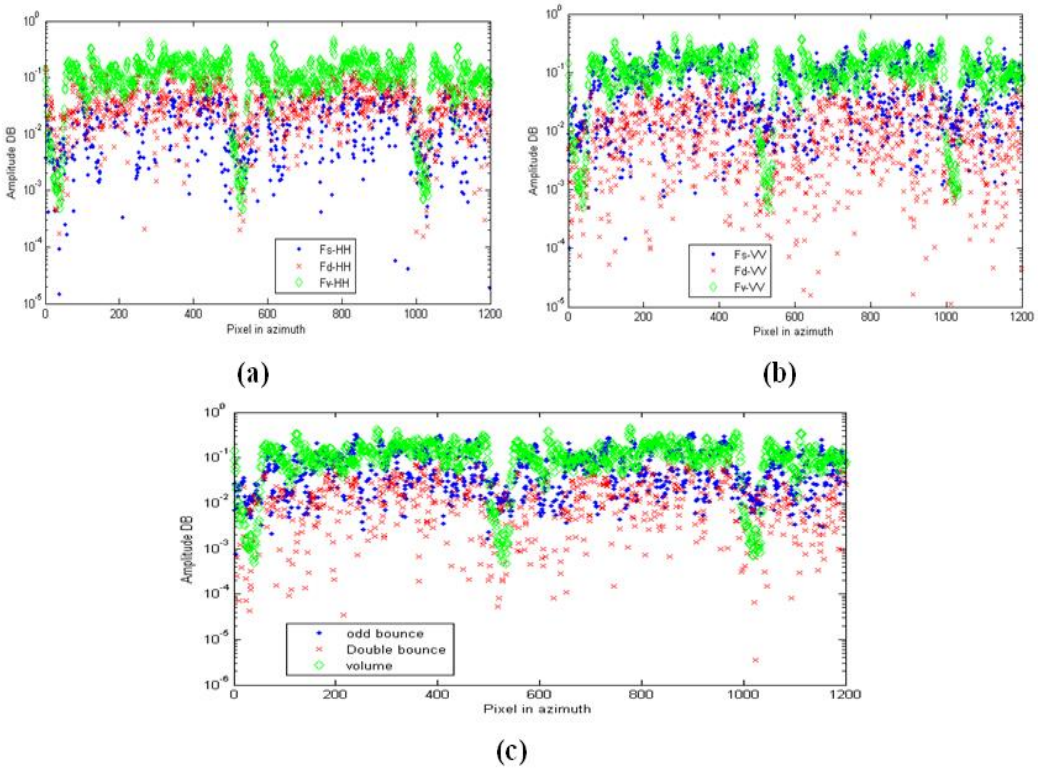

Figure 9. Amplitude contributions of the three scattering mechanisms to the (a) HH, (b) VV cross correlation and (c) to the total power provided by proposed algorithm for both ends of the baseline

Results for the amplitude of the three scattering contributions reveal that the volume scattering dominates for the HH and VV channels except for pixels around 10, 550 and 1100 according to agricultural areas see Figure 9(a) and (b). The double bounce mechanism is relatively high for the HH correlation but it is not dominant due to the relative roughness of terrain. Result from the proposed algorithm for both ends of the baseline is shown in Figure 9(c). It is shown that, there are no noticeable differences with two above cases, as expected. As seen, the volume contribution mostly dominates the response in the forest area, whereas the double-bounce contribution is about 1-5 dB below the volume respond to forest areas. When the interferometric information is considered, the volume contribution is obtained by the proposed algorithm which is slightly different when compared with volume contribution is achieved by Freeman-Durden decomposition for PolSAR image. Differences between both approaches become more evident at the agricultural area, specially, within azimuth intervals 230-250, 600-620 and 1100-1130. In the Freeman-Durden decomposition, the magnitude of volume and single bounce within these areas are nearly equal.

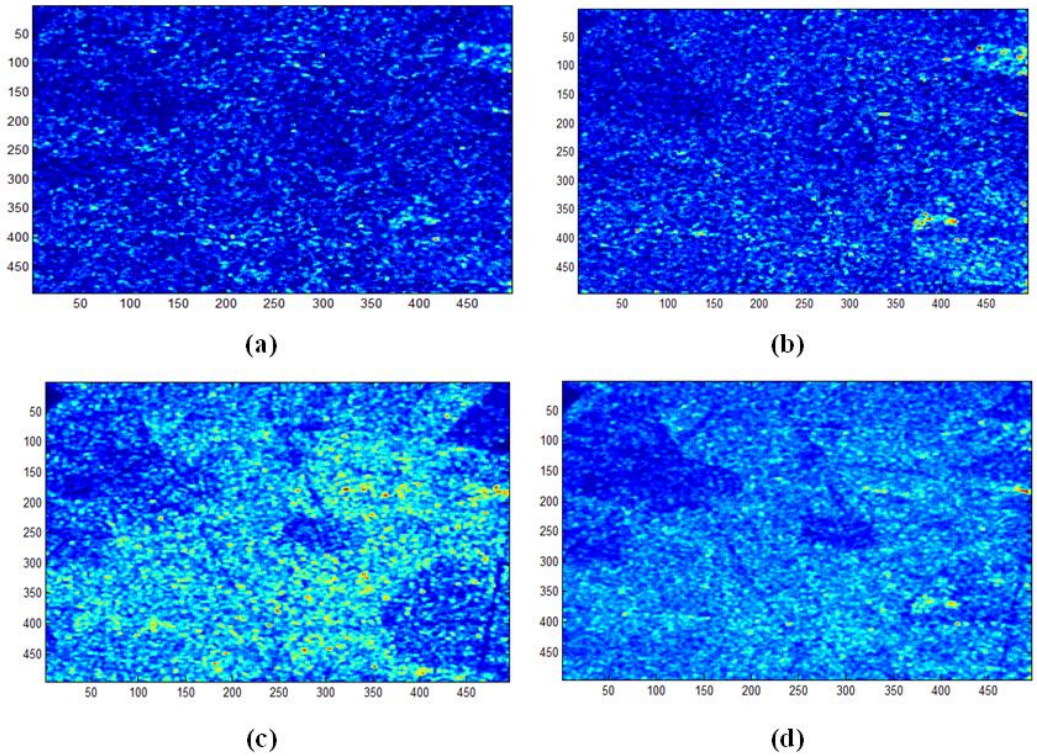

Figure 10. Results of the adaptive model-based decomposition (a) power image of PS (b) s power image of PD (c) power image of PV and (d) proposed decomposition algorithm for test site

Figure 10(a), (b) and (c) show the decomposed power image of odd-bounce (PS), double-bounce (PD) and volume scattering (PV) of the data by the proposed algorithm, respectively. In these figures, we do not observe negative power component, this means that power of volume scattering component is not overestimated. This is caused by the selected fit parameters for volume scattering covariance matrix and ambiguity reduction for scattering model decomposition. Comparing Figure 10 with Figure 7(a), we found out that, the double bounce scattering component in boundary forest and road areas are stronger than those of the forest and agricultural areas. Figure 10(d) shows the decomposition result of the adaptive model-based decomposition approach. The bold blue areas in the upper left and center correspond to agricultural, which shows that the single scattering is prominent. The light blue areas correspond to forest, indicating that the volume scattering is prominent.

Figure 11 shows a three dimensional perspective of the estimated height by the proposed algorithm. In this figure it is shown that almost the forest height is located in the range between 12m and 18m. The forest height estimation at some pixels is overestimated less than 30m. The real effective tree height will be higher than these values so we can say that the results are acceptable

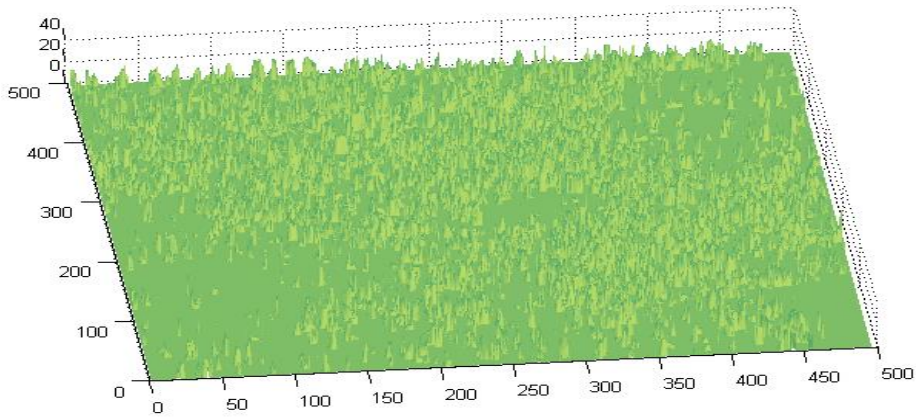

Figure 11. 3-D view of forest height

5. Conclusions

An adaptive model-based decomposition technique based on the cross correlation covariance matrix is proposed for polarimetric SAR interferometric data, which is intended to be applied to the general conditions, including both the non-reflection symmetry case and the reflection symmetry condition. In this paper, an accuracy enhancement method of vegetation height estimation using the adaptive model-based decomposition technique and coherence amplitude algorithm has been proposed. By using the proposed method we can not only obtain relative accuracy for height estimation but also estimate power contribution of each scattering component in each patch and on showing a general volume scattering component suitable to both symmetry and non-symmetry media. Simulated and spaceborne data have been used for testing the proposed algorithm and its potential has been analyzed also in comparison with the ESPRIT method for height estimation. These preliminary results show that the proposed model is effective for analysis of forest areas with PolInSAR image. Experimental results indicate that vegetation parameters can be retrieved directly and accurately by the fusion of these two approaches. In the future, more experiments using different data of different fields will be done and the enhancement performance of proposed algorithm will be studied.

Acknowledgments

This paper is a revised and expanded version of a paper entitled “Forest height estimation from PolInSAR image using adaptive decomposition”, presented at 11th International Conference on Signal Processing, Beijing, China, 2012 October 21-25.

References

[1] S. R. Cloude and K. P. Papathanassiou, “Polarimetric SAR interferometry”, IEEE Transaction on Geoscience and Remote Sensing, vol. 36, no. 5, **(1998)**, pp. 1551-1556.
[2] A. Freeman and S. L. Durden, “A three component scattering model to describle polarimetric SAR data”, IEEE Transaction on Geoscience and Remote Sensing, vol. 36, no. 3, **(1998)**, pp. 963-973.
[3] H. Yamada, M. Yamazaki and Y. Yamaguchi, “On scattering model decomposition of PolSAR and its application to ESPRIT-base Pol-InSAR”, Proceeding of 6th European Conference on Synthetic Aperture Radar, **(2006)** May 16-18, Dresden, Germany.

[4] J. D. Ballester-Bermand and J. M. Lopez-Sanchez, "Applying the Freeman-Durden decomposition concept to polarimatric SAR interferometry", IEEE Transaction on Geoscience and Remote Sensing, vol. 48, no. 1, **(2010)**, pp. 466-479.
[5] M. Arri, J. VanZyl and Y. Kim, "A general characterization for polarimetric scattering from vegetation canopies", IEEE Transaction on Geoscience and Remote Sensing, vol. 48, no. 9, **(2010)**, pp. 3349-3357.
[6] M. Arri, J. VanZyl and Y. Kim, "Adaptive model-based decomposition of polarimetric SAR covariance matrix", IEEE Transaction on Geoscience and Remote Sensing, vol. 49, no. 3, **(2011)**, pp. 1104-1113.
[7] O. Antropov, Y. Rauste and T. Hame, "Volume scattering modeling in PolSAR decompositions: study of ALOS PALSAR data over Boreal forest", IEEE Transaction on Geoscience and Remote Sensing, vol. 49, no. 10, **(2011)**, pp. 3838-3848.
[8] S. R. Cloude, "Polarisation application in remote sensing", Oxford University Press, NewYork, **(2009)**, pp. 284-339.
[9] Y. Yamaguchi, T. Moriyama, M. Ishido and H. Yamada, "Four component scattering model for polarimetric SAR image decomposition", IEEE Transaction on Geoscience and Remote Sensing, vol. 43, no. 8, **(2005)**, pp. 1699-1706.
[10] S. R. Cloude and K. P. Papathanassiou, "Three-stage inversion process for polarimetric SAR interferometric", IEE Proceedings Radar, Sonar and Navigation, vol. 150, Issue 3, **(2003)**, pp. 125-134.
[11] J. J. vanZy, M. Arri and Y. Kim, "Model-based decomposition of polarimetric SAR covariance matrices constrained for nonnegative eigenvalues, IEEE Transaction on Geoscience and Remote Sensing", vol. 49, no. 9, **(2011)**, pp. 3452-3459.
[12] S. R. Cloude and E. Pottier, "A review of target decomposition theorems in rasar polarimetry", IEEE Transaction on Geoscience and Remote Sensing, vol. 34, no. 2, **(1996)**, pp. 498-518.
[13] T. Mette, K. Papathanassiou and I. Hanjnsek, "Biomass estimation from polarimetric SAR interferometry over heterogeneous forest terrain", Proceeding of International Geoscience and Remote Sensing Symposium, vol. 1, **(2004)** September 20-24, pp. 510-514, Anchorage, Alaska.
[14] C. L. Martinez, X. Fabregas and L. Pipia, "Forest parameter estimation in the PolInSAR context employing the multiplicative-additive speckle noise model", Journal of Photogrammetry and Remote Sensing, vol. 66, **(2011)**, pp. 597-607.
[15] K. P. Papathanassiou and S. R. Cloude, "Single-baseline Polarimetric SAR interferometry", IEEE Transaction on Geoscience and Remote Sensing, vol. 39, **(2001)**, pp. 2352-2363.
[16] H. Yamada, Y. Yamaguchi, Y. Kim, E. Rodriguez and W. M. Boener, "Polarimetric SAR interferometry for forest analysis based on the ESPRIT algorithm", IEICE Transaction on Electron, vol. E 84-C, no. 12, **(2001)**, pp. 1917-2014.
[17] R. N. Treuhaft and P. Siqueria, "Vertical Structure of vegetated Land Surface from interferometric and polarimetric Radar", Radio Science, vol. 35, no. 1, **(2000)**, pp. 141-177.
[18] T. Mette, "Forest Biomass Estimation from Polarimetric SAR interferomtry", Ph.D dissertation, Techniche University München, Germany, **(2007)**.
[19] H. Yamada, Y. Yamaguchi, E. Rogriguez, Y. Kim and W. M. Boerner, "Polarimetric SAR interferometry for forest canopy analysis by using the super-resolution method", Proceeding of IEEE International Geoscience and Remote Sensing Symposium, **(2001)** July 9-13, pp. 1101-1103, Sydney, Ausralia.
[20] M. L. Williams, "PolSARproSim: A coherent, Polarimetric SAR simulation of Forest for PolSARPro", http//earth.eo.esa.int/polsarpro/SimulatedDataSources.html, **(2006)**.
[21] N. P. Minh, B. Zou and C. Yan, "Forest Height Estimation From PolInSAR Image Using Adaptive Decomposition Method", Proceeding of 11th International conference image processing, **(2012)** October 21-25, pp. 1830-1834, Beijing, China.

Authors

Nghia Pham Minh

Male, was born in 1980. He received the B.S., M.S. degrees from the Le Qui Don Technical University, Hanoi, Vietnam, in 2005 and 2008, respectively. Now he is pursuing Ph.D. degree in School of Electronics and Information Technology at Harbin Institute of Technology (HIT), Harbin, China. He currently focuses on synthetic aperture radar (SAR) image processing, polarimetric SAR, polarimetric SAR interferometry.

Bin Zou

Male, was born in 1968. He received the B.S. degree in electronic engineering from the Harbin Institute of Technology (HIT), Harbin, China, in 1990, the M.S. degree in space studies from the International Space University, Strasbourg, France, in 1998, and the Ph.D. degree in information and communication engineering from HIT, in 2001.

He was a Visiting Scholar in University of Manitoba, Winnipeg, Canada, from Oct. 2003 to Oct. 2004. He is currently a Professor and Vice Head of the Department of Information Engineering, School of Electronics and Information Technology, HIT. He currently focuses on synthetic aperture radar (SAR) image processing, polarimetric SAR, polarimetric SAR interferometry, hyperspectral imaging and data processing.